GIANI: open-source software for automated analysis of 3D microscopy images

David J. Barry[1*], Claudia Gerri[2], Donald M. Bell[1], Rocco D'Antuono[1], Kathy K. Niakan[2]

1 Crick Advanced Light Microscopy, Francis Crick Institute, London, NW1 1ST, UK

2 Human Embryo and Stem Cell Laboratory, Francis Crick Institute, London, NW1 1ST, UK

* david.barry@crick.ac.uk

Abstract

The study of cellular and developmental processes in physiologically relevant three-dimensional (3D) systems facilitates an understanding of mechanisms underlying cell fate, disease and injury. While cutting-edge microscopy technologies permit the routine acquisition of 3D datasets, there is currently a lack of user-friendly, open-source software to analyse such images. Here we describe GIANI (djpbarry.github.io/Giani), new software for the analysis of 3D images, implemented as a plugin for the popular FIJI platform. The design primarily facilitates segmentation of nuclei and cells, followed by quantification of morphology and protein expression. GIANI enables routine and reproducible batch-processing of large numbers of images and also comes with scripting and command line tools, such that users can incorporate its functionality into their own scripts and easily run GIANI on a high-performance computing cluster. We demonstrate the utility of GIANI by quantifying cell morphology and protein expression in mouse early embryos. More generally, we anticipate that GIANI will be a useful tool for researchers in a variety of biomedical fields.

Introduction

The ability to routinely acquire multi-dimensional datasets with modern microscopy techniques is transforming, among other fields, cell biology, developmental biology and cancer research. There has long been an acceptance that two-dimensional (2D) cell cultures may not accurately recreate behaviours found in complex, three-dimensional (3D) *in vivo* environments [1]. Commonly-used 3D culture formats include, but are not limited to, populations of single cells in organotypic matrices, spheroid models, tissue sections or

whole embryos and organisms.

However, the development of user-friendly software for the quantitative analysis of such data has not kept pace with imaging advances [2]. This presents an obvious challenge - how does one quantitatively analyse these datasets in a routine manner? Manual annotation of such data is not feasible, due to the time required to do so. Commercial packages, such as Imaris (Bitplane) and Vison4D (Arivis) provide excellent visualisation functionality and are also equipped with analysis tools. However, licenses for such software are expensive and they also rely on their own proprietary file formats. Furthermore, the closed-source nature of such software prevents detailed interrogation of specific calculations and processes.

There are numerous excellent, freely-available bioimage analysis tools in the open source domain. However, their support for 3D analysis is either limited (for example, several CellProfiler [3] modules are not yet compatible with 3D images) or challenging to execute and/or automate for the uninitiated (FIJI [4], Icy [5]). This can lead to undesirable compromises being made, such as 2D slices from a 3D volume being analysed individually, blinding the analysis to information in adjacent slices. Alternatively, 3D data may be compressed into 2D via projection, which, consequently, artificially reduces distances between objects. A number of very useful open-source MATLAB (MathWorks, Cambridge, UK) -based tools have also been implemented, most notably MINS, which has been effectively used to analyse embryo datasets [6] and LOBSTER [7]. However, these require the purchase of a MATLAB license and active maintenance of the code by the developers to avoid problems with backwards compatibility in newer versions of MATLAB.

We have therefore developed GIANI (https://djpbarry.github.io/Giani), a

user-friendly, generally-applicable, open source tool, implemented as a plugin for the widely-used image analysis platform, FIJI. With an emphasis on detection and segmentation of cells in 3D microscopy images, GIANI has been implemented specifically with batch-processing and minimal user interaction in mind. While an understanding of fundamental concepts of bioimage analysis is beneficial, GIANI has been implemented in a wizard format to facilitate use by non-specialists and is fully documented (https://github.com/djpbarry/Giani/wiki). Analysis protocols may be reproduced by loading a single, small parameter file.

The utility of GIANI is illustrated here using two examples. In the first, we generated a series of simulated datasets to evaluate the accuracy of segmentations produced by GIANI using known "ground truths". In the second proof-of-concept we use a series of mouse preimplantation embryo datasets and demonstrate the ability of GIANI to detect variations in morphology and protein expression in different experimental conditions. It should be noted that GIANI can be used to quantify 3D images from a range of cellular and developmental contexts and we anticipate that it will be a useful tool to automate quantification of a wide variety of complex imaging data.

Materials and methods

Simulated data generation

Simulated embryos were generated using an extension of a previously described method [8]. Simulated nuclei positions were generated as previously described [8], then cell membranes were approximated using a Euclidean Distance Map constructed around nuclei. The simulated images were then convolved with a Gaussian point-spread function, sub-sampled and noise added

from a gamma distribution. The complete code for simulated image generation is available on GitHub (https://github.com/djpbarry/Embryo-Generator).

Metrics for segmentation quality assessment

We calculated the cell count error E_c, as

$$E_c = |N_g - N_{gt}| \tag{1}$$

where N_{gt} is the actual number of cells present in a simulated embryo and N_g is the number counted by GIANI. Nuclear (E_{nl}) and cell (E_{cl}) centroid localisation errors were calculated based on the euclidean distance between the known ground truth centroids and the centroids of the segmentations produced by GIANI.

Mouse zygote collection

Four- to eight-week-old (C57BL6 $\times$ CBA) F1 female mice were super-ovulated using injection of 5 IU of pregnant mare serum gonadotrophin (PMSG; Sigma-Aldrich). Forty-eight hours after PMSG injection, 5 IU of human chorionic gonadotrophin (HCG; Sigma-Aldrich) was administered. Superovulated females were set up for mating with eight-week-old or older (C57BL6 $\times$ CBA) F1 males. Mice were maintained on a 12 h light–dark cycle. Mouse zygotes were isolated in EmbryoMax FHM mouse embryo media (Sigma-Aldrich; MR-122-D) under mineral oil (Origio; ART-4008-5P) and cumulus cells were removed with hyaluronidase (Sigma-Aldrich; H4272). All animal research was performed in compliance with the UK Home Office

Licence Number 70/8560.

Mouse embryo culture

Mouse embryos were cultured in drops of pre-equilibrated Global medium (LifeGlobal; LGGG-20) supplemented with 5 mg/ml protein supplement (LifeGlobal; LGPS-605) and overlaid with mineral oil (Origio; ART-4008-5P). Preimplantation embryos were incubated at 37°C and 5.5% CO_2 and cultured up to the day of analysis.

Inhibitor treatment

Inhibitor experiment was performed as previously described [9]. Briefly, the aPKC inhibitor CRT0276121 (Cancer Research Technology LTD) was dissolved in DMSO to 10 mM stock concentration and diluted to the optimal concentration of 8 μM in pre-equilibrated embryo culture media. Control mouse embryos were developed in pre-equilibrated media where the same amount of DMSO was added.

Immunofluorescence

Embryos were fixed with freshly prepared 4% paraformaldehyde in PBS that was pre-chilled at 4°C. Embryo fixation was performed for 20 min at RT and then the embryos were transferred through 3 washes of 1X PBS with 0.1% Tween-20 to remove residual paraformaldehyde. Embryos were permeabilized with 1X PBS with 0.5% Triton X-100 and then blocked in blocking solution (3% BSA in 1X PBS with 0.2% Triton X-100) for 2 h at RT on a rotating shaker. Then, embryos were incubated with primary antibodies (listed in Table 1) diluted in blocking solution overnight at 4°C on rotating shaker.

Table 1. Primary antibodies used in this study and the dilution at which they were used.

Antibody	Supplier	Catalogue Number	Dilution
YAP1	Abnova	H00010413-M01	1:50
GATA3	R&D	AF2605	1:200
E-CADHERIN	Life Technologies	131900	1:400

The following day, embryos were washed in 1X PBS with 0.2% Triton X-100 for 20 min at RT on rotating shaker and then incubated with secondary antibodies diluted in blocking solution for 1 h at RT on rotating shaker in the dark. Next, embryos were washed in 1X PBS with 0.2% Triton X-100 for 20 min at RT on rotating shaker. Finally, embryos were placed in 1X PBS with 0.1% Tween-20 with Vectashield with DAPI mounting medium (Vector Lab; H-1200) (1:30 dilution). Embryos were placed on μ-Slide 8 well dishes (Ibidi; 80826) for confocal imaging.

Image Acquisition

All images were acquired on a Leica SP5 laser scanning confocal microscope using a Leica 1.3 NA 63x HCX PL APO CS glycerol objective and a voxel size of approximately 0.1 x 0.1 x 1.0 μm in x, y and z, respectively.

Software

GIANI was written using Java 8 as a plug-in for FIJI [4], making extensive use of the underlying FIJI and ImageJ [10] libraries. A number of other open-source projects are leveraged. Reading of image data is facilitated by interfacing to Bio-Formats [11]. Detection of nuclear blobs makes use of either TrackMate's spot detector [12] or FeatureJ (https://imagescience.org/meijering/software/featurej). Segmentation of cells

and nuclei takes advantage of the marker-controlled watershed functionality in MorphoLibJ [13] and 3D Image Suite [14]. The browsing of results is based upon the 3D Region of Interest (ROI) Manager from 3D Image Suite. Complete source code, documentation and test data are available online (https://djpbarry.github.io/Giani).

Results & Discussion

Software implementation

The design philosophy behind GIANI is inspired by CellProfiler. It is assumed that the user wishes to detect "primary objects" of some sort (typically cell nuclei), followed by the subsequent segmentation of "secondary objects" (typically cells) and then wishes to measure either the morphology of said objects, or the expression of a fluorescent signal within these objects. The principal difference in the case of GIANI is that, in order to facilitate ease of use, the order of steps in the pipeline is fixed, although some flexibility is present where necessary (Fig 1).

Analysis of simulated embryos

To first validate the performance of GIANI, we generated a series of 189 "simulated embryos" exhibiting different levels of signal-to-noise ratio and cell density (Fig 2A). Simulated data has the significant advantage of having a known "ground truth" (Fig 2B). That is, because the images are generated artificially, we know what the "correct" segmentation should look like. This permits us to compare the segmentation results generated with any piece of analysis software with the known "true" values.

Fig 1. Overview of GIANI's operation All embryo images represent a single slice of a 3D stack. A: The GIANI Graphical User Interface. B: An example dataset, consisting of a 3D stack image of a mouse embryo showing DAPI (blue), E-Cadherin (red) and GATA-3 (green). C: Positions of nuclei are first approximated using a blob detector, which provides an estimate of each nuclear centroid. D: Prior to complete segmentation, the nuclear image stack is Gaussian filtered in three dimensions. E: Complete segmentation of the nuclei is achieved using a marker-controlled watershed approach, with the filtered image from D serving as the input and centroids from C serving as the markers. The extent of the nuclei is based on an intensity threshold, calculated using one of FIJI's in-built thresholding algorithms, specified by the user. F: Prior to conducting cell segmentation, the image channel delineating cells is Gaussian filtered in three dimensions. Either a volume marker or membrane marker can be used, but the latter will result in more accurate segmentation. G: Cell segmentation is achieved using a marker-controlled watershed approach, with the filtered image from F serving as the input and nuclei segmentations from E serving as the markers. The extent of the cells is again based on an intensity threshold, calculated using one of FIJI's thresholding algorithms. H: Quantification of fluorescence intensities in any number of user-specified channels is performed using the segmentations from E and G. Results are generated for each nucleus, cell and cytoplasmic region in each input stack. I: Once a batch analysis has been completed, segmentations and associated fluorescence quantifications can be explored using the provided results browser.

Fig 2. Validation of GIANI using simulated embryo data. In each of the heat maps, a single tile represents the average of three simulated embryos. A: A 2D slice of an exemplar 3D simulated embryo. B: The ground truth segmentation of 'A'. C - H: Absolute errors in cell counts (E_c, calculated according to Eq 1), nuclear centroid localisation error (E_{nl}) and cell centroid localisation error (E_{cl}) produced by GIANI for simulated embryos with the indicated number of cells and signal-to-noise ratios (SNR). Results were obtained using either GIANI's basic (C - E) or advanced (F - H) nuclear detector.

The number of false positives and false negatives produced by GIANI is consistently extremely low, although cell count errors do generally increase with cell density and decreasing signal-to-noise ratio (SNR; Fig 2C, F). At high SNR and low cell densities, GIANI localises nuclei to within approximately 600 nm of their true positions (Fig 2D, G). Even at high cell densities and low SNR, this error never exceeded 1 μm (the simulated nuclei are ellipsoidal with axis

dimensions of approximately 10.0 x 7.5 x 7.5 μm). In addition to nuclear localisation error, we also quantified the cell centroid localisation error on a per cell basis (Fig 2E, H).

The accurate characterisation of a multi-cellular dataset, such as an embryo, is fundamentally dependent on the correct identification and segmentation of nuclei. While GIANI presently employs generic blob detectors for this purpose, which is similar to other previously-described methods [6], other approaches are also possible [15–19]. It is intended that some alternative functionality will be added in future releases. In particular, incorporating machine-learning classifiers trained with, for example, Weka [20] or Ilastik [21] will be prioritised.

In addition to the convolution of the ground truth data, the simulation process also takes into consideration depth of slices within a sample when modelling fluorescent intensity - deeper slices will be more prone to scattering effects and therefor exhibit lower intensity. This means that finding a single global thresholding strategy that does not under-segment the dimmer cells while also not over-segmenting the brighter cells is challenging. Taking all this into consideration, any metric used to assess the accuracy of cell segmentations will have its limitations.

There are strategies that could be employed to mitigate against these factors. For example, some form of adaptive thresholding, whereby the intensity threshold changes according to z-location, could be used. However, while an optimal adaptive thresholding strategy could be found for a given dataset (such as the simulated data used in this study), implementing a universally-applicable strategy would be difficult. One of the principle design aims of GIANI was simplicity of use, which does not allow for the incorporation of a variety of case-specific segmentation approaches.

Analysis of mouse embryos

We subsequently applied GIANI to the analysis of two populations of mouse preimplantation embryos at the morula stage, one control and one treated with a small molecule inhibitor [9]. At this stage, two distinct cell populations are discernible: inner and outer cells. In subsequent cell divisions, a blastocyst is formed, whereby the inner cells give rise to an inner cell mass (ICM), and the outer cells become the trophectoderm (TE), a polarized epithelium that will form fetal components of the placenta [22].

At the morula stage, inner and outer cells display different polarisation states, which influence their cell fate acquisition. The outer cells acquire an apical domain, enriched with the atypical protein kinase C (aPKC) [23]. In the polar outer cells, aPKC prevents activation of downstream Hippo pathway kinases, Large tumor suppressor kinases 1/2 (LATS1/2) [24]. Consequently, in outer cells, YAP1 accumulates in the nucleus, where it promotes the expression of GATA3 [25]. In contrast, in the apolar inner cells, the activation of the Hippo pathway results in YAP1 cytoplasmic retention, thus maintaining the inner cells in an unspecified state [24, 26, 27].

We therefore divided cells within each embryo into an ‘inner’ and ‘outer’ population (Fig 3A, B). This division is based on the distance of the detected nuclear centroid from the embryo centroid. A cell was classified as ‘inner’ if the following condition held true:

$$\frac{D_i}{D_m} < D_T \tag{2}$$

where D_i is the Euclidean distance of cell i from the embryo centroid, D_m is the

maximum Euclidean distance from any cell in the same embryo to the embryo centroid and D_T is an arbitrarily set distance threshold. For the purposes of this study, we chose a value of 0.5 for D_T - it was found that modifying this value slightly ($\pm 10\%$) did not significantly impact the results (data not shown). The embryo centroid was calculated as the average of all nuclear centroids.

Fig 3. GIANI reveals differences in morphology and protein expression in mouse embryos. All box plots show the median and inter-quartile range, with the whiskers extending 1.5 times the inter-quartile range from the 25th and 75th percentiles. Unless otherwise stated, each dot represents a single cell. A. Illustration of the division of embryo cells into 'outer' (red) and 'inner' (green) sub-populations. The embryo centroid is indicated by the white square. The blue circle has radius D_m (see Eq 2) and indicates the distance from the embryo centroid to the most distant nucleus centroid. The radius of the yellow circle is $D_T \times D_m$ (Eq 2). B. The number of cells in each embryo divided into outer and inner sub-populations using a value of 0.5 for D_T in control embryos. Each dot represents a single embryo ($n_{control} = 18$). C: Volume of nuclei in inner/outer populations in control embryos. D: Volume of cells in inner/outer populations in control embryos. E: Ratio of cell-to-nuclear volume in inner and outer cells in control embryos. F: Nuclear/cytoplasmic ratio of YAP1 expression in control embryos. G: Difference in expression profiles of nuclear GATA3 expression, normalised to DAPI, in control and treated embryos ($n_{treated} = 20$). H: Difference in nuclear/cytoplasmic ratiometric expression profiles of YAP1 in control and treated embryos.

GIANI shows differences in cell morphology, YAP1 and GATA3 expression within inner and outer cells in control embryos

We then applied GIANI to detect variations in morphology and protein expression in mouse preimplantation embryos. We began with a morphological analysis of cells in control embryos. While no significant difference was found between median nuclear volumes in inner and outer cell populations (Fig 3C; $p = 0.861$, Wilcoxon rank sum test), a difference in size distributions is evident. A difference in median cell volume between the two populations was also identified, although it fell slightly short of being statistically significant

(Fig 3D; $p = 0.069$). However, a comparison of cell-to-nucleus volume ratios revealed a significant difference between median values, with outer cells having a proportionately greater cytoplasmic volume than inner cells (Fig 3E; $p < 0.001$). We also confirmed previous analysis of YAP1 translocation [28], illustrating that nuclear localisation is significantly higher in outer versus inner cells (Fig 3F; $p < 0.001$). Similarly, GATA3 expression was shown to be higher in outer compared to inner cells (Fig 3G; $p < 0.0001$).

GIANI reveals differences in YAP1 and GATA3 expression in mouse embryos after pharmacological treatment

To further demonstrate the utility of GIANI, we sought to analyse GATA3 and YAP1 expression after treating mouse embryos with a small molecular inhibitor against aPKC, the upstream regulator of YAP1 and GATA3. The aPKC inhibitor, CRT0276121, has previously been confirmed to specifically inhibit aPKC in various biological and cellular contexts [29–31]. Specifically, in mouse pre-implantation embryos, aPKC inhibition has been recently shown to efficiently abrogate YAP1 and GATA3 expression in outer cells [9].

Expression of GATA3 in the nucleus (normalised to DAPI to correct for diminished signal intensity with increasing sample depth) was found to be similarly low in the inner cells of both control and treated embryos (Fig 3G; $p = 0.841$). However, GATA3 expression in outer cells was found to be significantly lower in the treated embryos relative to the control group ($p < 0.002$). Normalised expression of GATA3 was also found to be significantly higher in outer cells of control embryos relative to their inner cells ($p < 0.001$), while the same was not true of treated embryos ($p = 0.171$). In addition, differences in distribution are evident between control and treated

embryos, with two distinct populations evident in both inner and outer cells in control populations (Fig 3G).

While no statistically significant difference in nuclear YAP1 expression (normalised to cytoplasmic expression) between control and treated cells were observed when comparing inner cells (Fig 3H; $p = 0.609$), a large difference was observed in outer cells ($p < 0.0001$). However, nuclear/cytoplasmic YAP1 expression was still higher in the outer cells of treated embryos versus inner ($p < 0.0001$). Altogether, this demonstrates that GIANI allows for the automated quantification of expression differences between cells following perturbation.

Future developments

Given the ongoing interest in studying cells in "native" 3D extracellular environments [32], future extension to the capabilities of GIANI will include the ability to analyse time-lapse data, as there is currently a lack of open source tools for the quantification of 3D cell migration [33]. The incorporation of additional functionality from TrackMate (and MaMuT [34] or Mastodon) will be explored to facilitate 3D cell tracking.

Future development will also include the replacement of the 3D ROI Manager interface for visualizing results with a new, custom-built interface. This will probably be replaced in a subsequent release with a new custom-built interface. At present, segmented objects are saved solely as FIJI ROI files, but it is intended that support for other formats (such as .stl, .ply, .obj and .x3d) will be added to allow the import of objects into a variety of different software.

More generally, with a view to improving and optimising performance, further use of ImgLib2 [35] will be incorporated in future releases. Taking

advantage of GPU acceleration is also an aim, most likely by exploiting CLIJ [36]. For this study, analysis of a single mouse embryo dataset (approx. 1024 x 1024 x 76 voxels) took approximately 5 minutes on a desktop PC (Intel Xeon E5-2630 v4, 32GB RAM) versus 10 minutes on a laptop (Intel Core i7-6600U, 16 GB RAM).

Conclusion

We have used GIANI to quantitatively analyse mouse embryos in 3D. This analysis has revealed differences in morphology and protein expression between different experimental conditions. Analysis of simulated ground truth data was used to confirm the validity of these results. Further development of GIANI is planned, with the specific aim of improving segmentations in noisy and dense fields of view, common in 3D images of cells. Extension to timelapse analysis is also planned. GIANI is freely available on GitHub (github.com/djpbarry/Giani) and we anticipate that it will be a useful resource for the community to perform routine, automated quantification of complex imaging data.

Acknowledgments

Thanks to Kurt Anderson for his constructive comments on the manuscript.

References

1. Duval K, Grover H, Han LH, Mou Y, Pegoraro AF, Fredberg J, et al. Modeling Physiological Events in 2D vs. 3D Cell Culture. Physiology. 2017;32(4):266–277.

2. Meijering E, Carpenter AE, Peng H, Hamprecht FA, Olivo-Marin JC. Imagining the future of bioimage analysis. Nature Biotechnology. 2016;34(12):1250–1255.

3. Lamprecht MR, Sabatini DM, Carpenter AE. CellProfiler™: free, versatile software for automated biological image analysis. BioTechniques. 2007;42(1):71–75.

4. Schindelin J, Arganda-Carreras I, Frise E, Kaynig V, Longair M, Pietzsch T, et al. Fiji: an open-source platform for biological-image analysis. Nature Methods. 2012;9:676.

5. de Chaumont F, Dallongeville S, Chenouard N, Hervé N, Pop S, Provoost T, et al. Icy: an open bioimage informatics platform for extended reproducible research. Nature Methods. 2012;9:690.

6. Lou X, Kang M, Xenopoulos P, Muñoz-Descalzo S, Hadjantonakis AK. A Rapid and Efficient 2D/3D Nuclear Segmentation Method for Analysis of Early Mouse Embryo and Stem Cell Image Data. Stem Cell Reports. 2014;2(3):382 – 397.

7. Tosi S, Bardia L, Filgueira MJ, Calon A, Colombelli J. LOBSTER: An environment to design bioimage analysis workflows for large and complex fluorescence microscopy data. Bioinformatics. 2019;.

8. Rajasekaran B, Uriu K, Valentin G, Tinevez JY, Oates AC. Object Segmentation and Ground Truth in 3D Embryonic Imaging. PLOS ONE. 2016;11(6):1–17.

9. Gerri C, McCarthy A, Alanis-Lobato G, Demtschenko A, Bruneau A, Loubersac S, et al. Initiation of a conserved trophectoderm program in human, cow and mouse embryos. Nature. 2020;.

10. Schneider CA, Rasband WS, Eliceiri KW. NIH Image to ImageJ: 25 years of image analysis. Nature methods. 2012;9:671–675.

11. Linkert M, Rueden CT, Allan C, Burel JM, Moore W, Patterson A, et al. Metadata matters: access to image data in the real world. The Journal of Cell Biology. 2010;189(5):777–782.

12. Tinevez JY, Perry N, Schindelin J, Hoopes GM, Reynolds GD, Laplantine E, et al. TrackMate: An open and extensible platform for single-particle tracking. Methods. 2017;115:80 – 90.

13. Legland D, Arganda-Carreras I, Andrey P. MorphoLibJ: integrated library and plugins for mathematical morphology with ImageJ. Bioinformatics. 2016;32(22):3532–3534.

14. Ollion J, Cochennec J, Loll F, Escudé C, Boudier T. TANGO: a generic tool for high-throughput 3D image analysis for studying nuclear organization. Bioinformatics. 2013;29:1840–1841.

15. Kostrykin L, Schnörr C, Rohr K. Globally optimal segmentation of cell nuclei in fluorescence microscopy images using shape and intensity information. Medical Image Analysis. 2019;58:101536.

16. Weigert M, Schmidt U, Haase R, Sugawara K, Myers G. Star-convex Polyhedra for 3D Object Detection and Segmentation in Microscopy; 2019.

17. Blin G, Sadurska D, Portero Migueles R, Chen N, Watson JA, Lowell S. Nessys: A new set of tools for the automated detection of nuclei within intact tissues and dense 3D cultures. PLOS Biology. 2019;17(8):1–29.

18. Caicedo JC, Goodman A, Karhohs KW, Cimini BA, Ackerman J, Haghighi M, et al. Nucleus segmentation across imaging experiments: the 2018 Data Science Bowl. Nature Methods. 2019;.

19. Yang L, Ghosh RP, Franklin JM, Chen S, You C, Narayan RR, et al. NuSeT: A deep learning tool for reliably separating and analyzing crowded cells. PLOS Computational Biology. 2020;16(9):1–20.

20. Arganda-Carreras I, Kaynig V, Rueden C, Eliceiri KW, Schindelin J, Cardona A, et al. Trainable Weka Segmentation: a machine learning tool for microscopy pixel classification. Bioinformatics. 2017;33(15):2424–2426.

21. Berg S, Kutra D, Kroeger T, Straehle CN, Kausler BX, Haubold C, et al. ilastik: interactive machine learning for (bio)image analysis. Nature Methods. 2019;.

22. Cockburn K, Rossant J. Making the blastocyst: lessons from the mouse. The Journal of Clinical Investigation. 2010;120(4):995–1003.

23. Plusa B, Frankenberg S, Chalmers A, Hadjantonakis AK, Moore CA, Papalopulu N, et al. Downregulation of Par3 and aPKC function directs cells towards the ICM in the preimplantation mouse embryo. Journal of Cell Science. 2005;118(3):505–515.

24. Hirate Y, Hirahara S, Inoue KI, Suzuki A, Alarcon VB, Akimoto K, et al. Polarity-dependent distribution of angiomotin localizes Hippo signaling

in preimplantation embryos. Current biology. 2013;23(23791731):1181–1194.

25. Ralston A, Cox BJ, Nishioka N, Sasaki H, Chea E, Rugg-Gunn P, et al. Gata3 regulates trophoblast development downstream of Tead4 and in parallel to Cdx2. Development. 2010;137(3):395–403.

26. Cockburn K, Biechele S, Garner J, Rossant J. The Hippo Pathway Member Nf2 Is Required for Inner Cell Mass Specification. Current Biology. 2013;23(13):1195 – 1201.

27. Frum T, Murphy TM, Ralston A. HIPPO signaling resolves embryonic cell fate conflicts during establishment of pluripotency in vivo. eLife. 2018;7(30526858):e42298.

28. Nishioka N, ichi Inoue K, Adachi K, Kiyonari H, Ota M, Ralston A, et al. The Hippo Signaling Pathway Components Lats and Yap Pattern Tead4 Activity to Distinguish Mouse Trophectoderm from Inner Cell Mass. Developmental Cell. 2009;16(3):398 – 410.

29. Kjær S, Linch M, Purkiss A, Kostelecky B, Knowles P, Rosse C, et al. Adenosine-binding motif mimicry and cellular effects of a thieno[2,3-d]pyrimidine-based chemical inhibitor of atypical protein kinase C isoenzymes. Biochemical Journal. 2013;451(2):329–342.

30. Rodriguez J, Peglion F, Martin J, Hubatsch L, Reich J, Hirani N, et al. aPKC Cycles between Functionally Distinct PAR Protein Assemblies to Drive Cell Polarity. Developmental Cell. 2020;42(4):400–415.e9.

31. Aguilar-Aragon M, Elbediwy A, Foglizzo V, Fletcher GC, Li VSW, Thompson BJ. Pak1 Kinase Maintains Apical Membrane Identity in Epithelia. Cell Reports. 2020;22(7):1639–1646.

32. Yamada KM, Sixt M. Mechanisms of 3D cell migration. Nature Reviews Molecular Cell Biology. 2019;.

33. Masuzzo P, Troys MV, Ampe C, Martens L. Taking Aim at Moving Targets in Computational Cell Migration. Trends in Cell Biology. 2016;26(2):88 – 110.

34. Wolff C, Tinevez JY, Pietzsch T, Stamataki E, Harich B, Guignard L, et al. Multi-view light-sheet imaging and tracking with the MaMuT software reveals the cell lineage of a direct developing arthropod limb. eLife. 2018;7:e34410.

35. Pietzsch T, Preibisch S, Tomančák P, Saalfeld S. ImgLib2—generic image processing in Java. Bioinformatics. 2012;28(22):3009–3011.

36. Haase R, Royer LA, Steinbach P, Schmidt D, Dibrov A, Schmidt U, et al. CLIJ: GPU-accelerated image processing for everyone. Nature Methods. 2020;17(1):5–6.

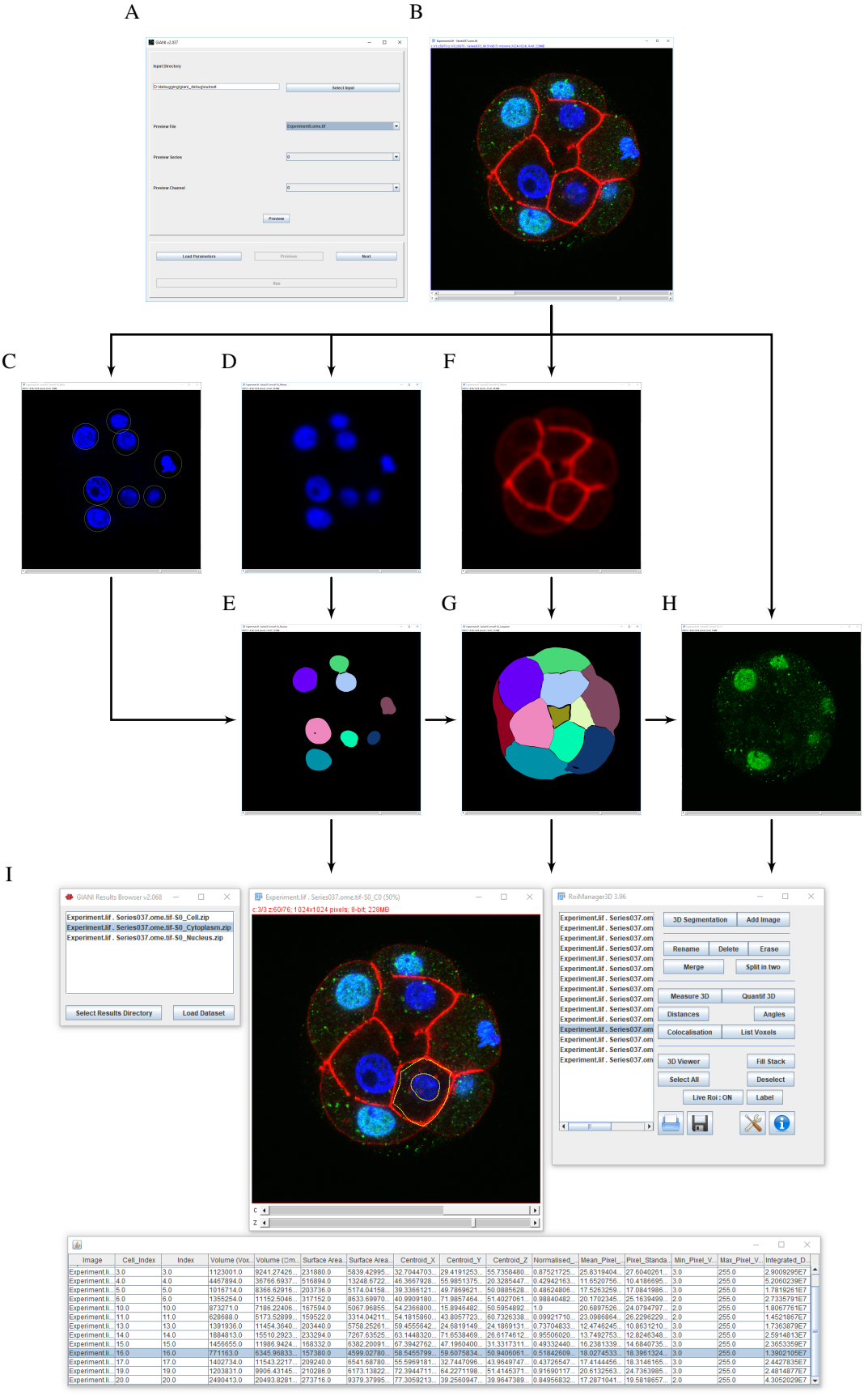

Figure 1

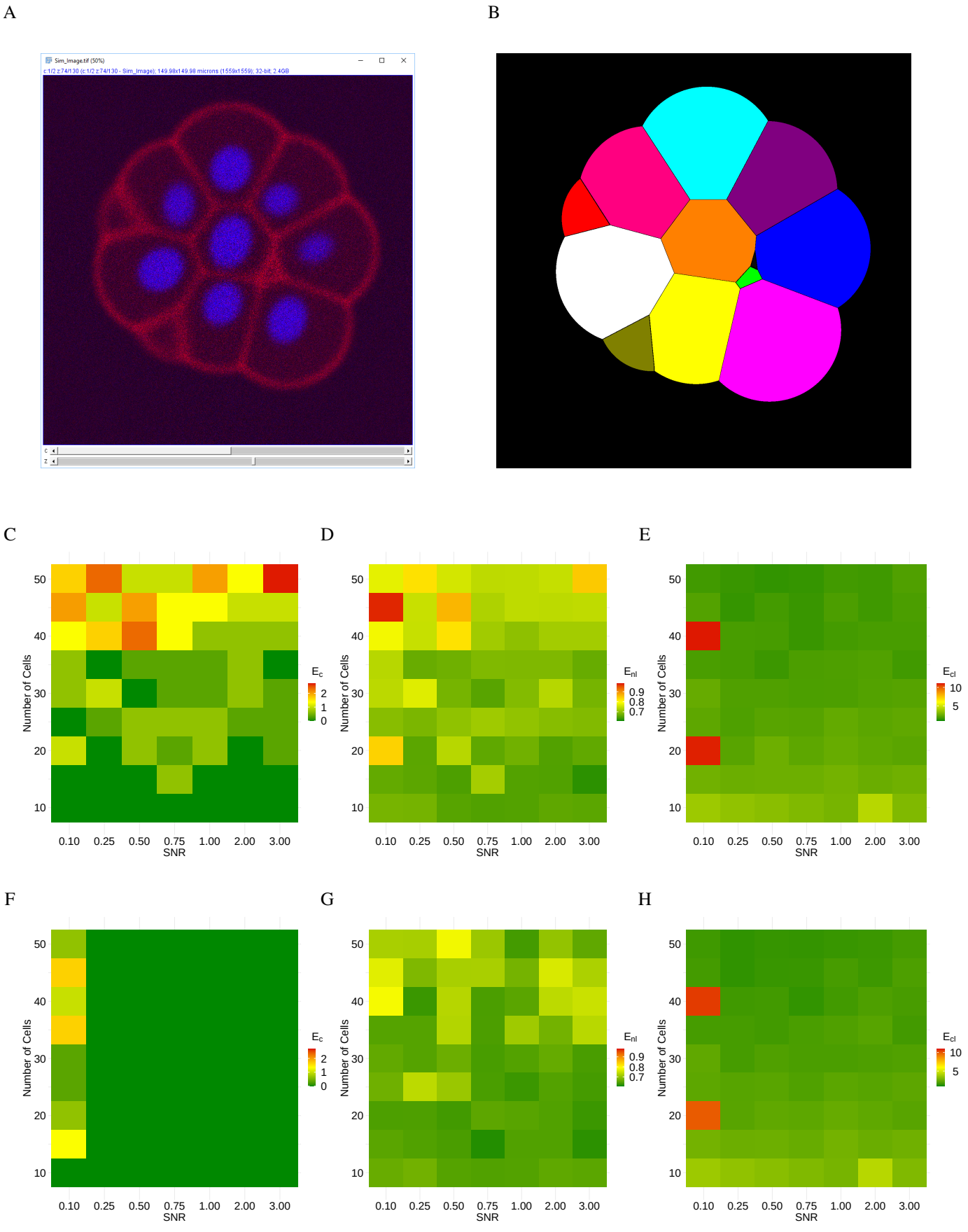

Figure 2

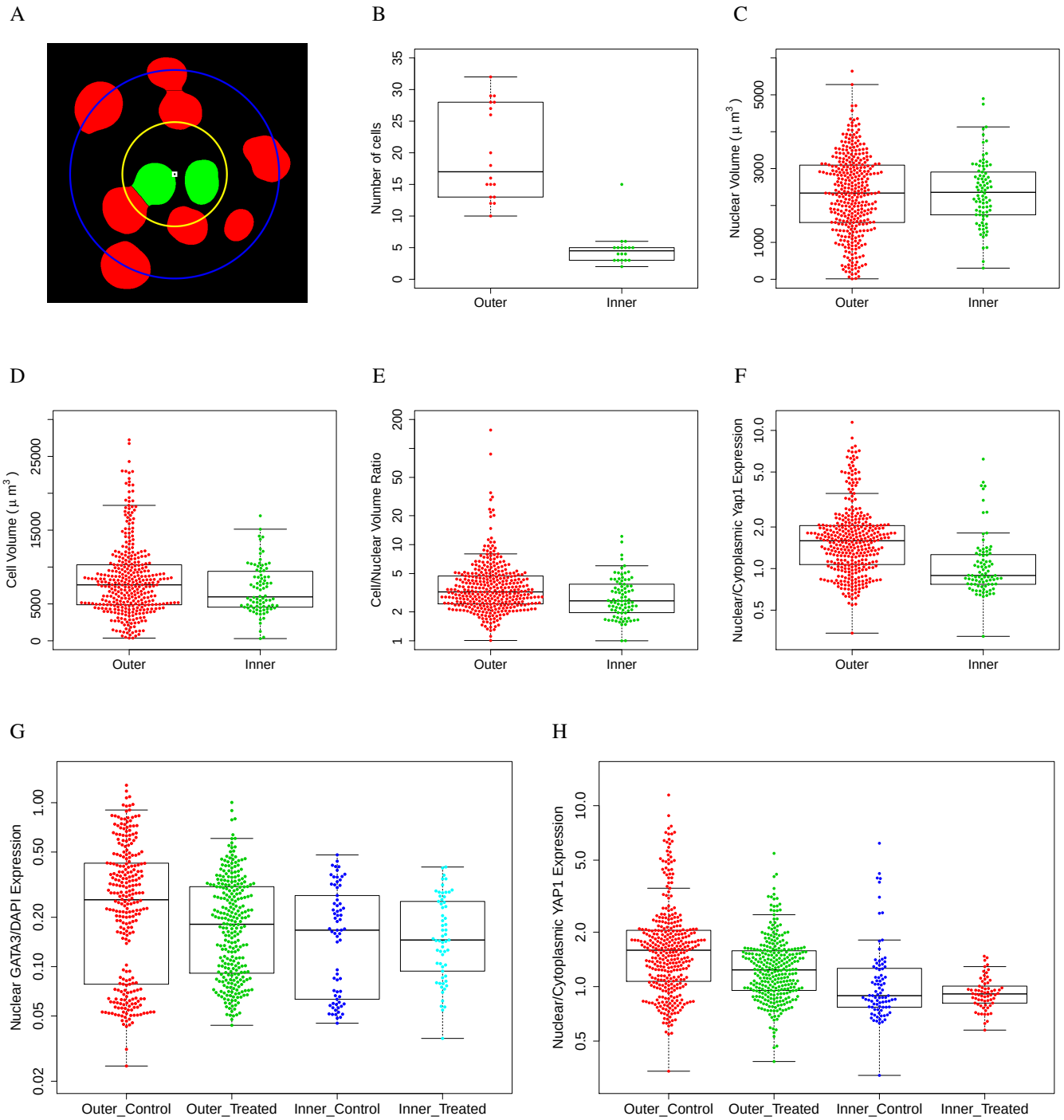

Figure 3